

Aligning Microscopic Vehicle and Macroscopic Traffic Statistics: Reconstructing Driving Behavior from Partial Data

Zhihao Zhang

*dept. Electrical and Computer Engineering
The Ohio State University
Columbus, USA
zhang.11606@osu.edu*

Chengyang Peng

*dept. Mechanical and Aerospace Engineering
The Ohio State University
Columbus, USA
peng.947@osu.edu*

Keith A. Redmill

*dept. Electrical and Computer Engineering
The Ohio State University
Columbus, USA
redmill.1@osu.edu*

Bowen Weng

*Department of Computer Science
Iowa State University
Ames, IA, USA
bweng@iastate.edu*

Abstract—A driving algorithm that aligns with good human driving practices, or at the very least collaborates effectively with human drivers, is crucial for developing safe and efficient autonomous vehicles. In practice, two main approaches are commonly adopted: (i) supervised or imitation learning, which requires comprehensive naturalistic driving data capturing all states that influence a vehicle’s decisions and corresponding actions, and (ii) reinforcement learning (RL), where the simulated driving environment either matches or is intentionally more challenging than real-world conditions. Both methods depend on high-quality observations of real-world driving behavior, which are often difficult and costly to obtain. State-of-the-art sensors on individual vehicles can gather microscopic data, but they lack context about the surrounding conditions. Conversely, roadside sensors can capture traffic flow and other macroscopic characteristics, but they cannot associate this information with individual vehicles on a microscopic level. Motivated by this complementarity, we propose a framework that reconstructs unobserved microscopic states from macroscopic observations, using microscopic data to anchor observed vehicle behaviors, and learns a shared policy whose behavior is microscopically consistent with the partially observed trajectories and actions and macroscopically aligned with target traffic statistics when deployed population-wide. Such constrained and regularized policies promote realistic flow patterns and safe coordination with human drivers at scale.

Index Terms—Cooperative Control, Autonomous Driving

I. INTRODUCTION

The ability to design driving algorithms that emulate human behavior and coordinate safely with human drivers depends in part on how driving data are collected and used. In practice, such data are organized at two complementary levels as shown

Zhihao Zhang and Keith A. Redmill are supported by Carnegie Mellon University’s Safety21 National University Transportation Center, which is sponsored by the US Department of Transportation under grants 69A3552344811/69A3552348316.

in Fig. 1. Microscopic data capture individually observed vehicle trajectories, control actions, and local surroundings using on-board sensors [1]–[4]. These data are the basis for supervised and imitation learning pipelines that fit a parameterized policy to map local observations to human-like actions [2], [5]–[10]. These approaches can produce highly interpretable and reactive policies. However, they critically rely on dense, high-resolution sensing that observes all relevant agents and typically require substantial, labor-intensive labeling [2], [11], [12]. Macroscopic data, on the other hand, consist of aggregated traffic statistics such as mean speed, flow, and density over space and time, typically obtained from infrastructure sensors such as cameras or loop detectors [13]. Such aggregates are widely available and are routinely used to calibrate or validate large-scale traffic simulators and reinforcement learning environments [7], [14], where background vehicles follow dynamics tuned to match observed flow patterns. While RL in these simulators can optimize long-term performance under challenging conditions, its fidelity is limited by how well the simulated population reproduces real macroscopic behavior and by the lack of direct association with individual human trajectories [15]–[17].

Methods built exclusively on microscopic trajectories from instrumented or connected vehicles can fit fine-grained state–action maps but suffer from limited coverage and missing population context, as such traces represent only a small fraction of the flow [18]–[22]. In contrast, methods calibrated solely on infrastructure aggregates (e.g., mean speed, flow, density) reproduce bulk trends yet cannot attribute behavior to individual agents, creating an identifiability gap in which multiple policies yield indistinguishable aggregates [23], [24].

Motivated by this complementarity, we propose a macro–micro integrated framework that reconstructs unob-

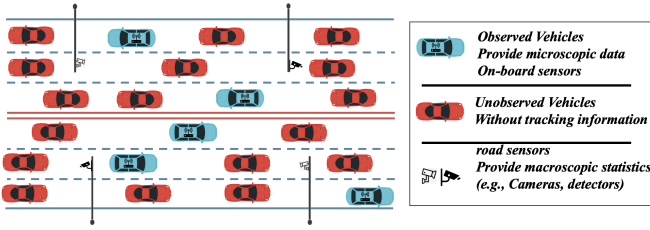


Fig. 1. Partially observed traffic setting. A small subset of instrumented vehicles (blue) provides microscopic trajectories and actions, while the remaining vehicles (red) are unobserved. Roadside sensors (e.g., cameras/detectors) supply macroscopic statistics for the whole stream

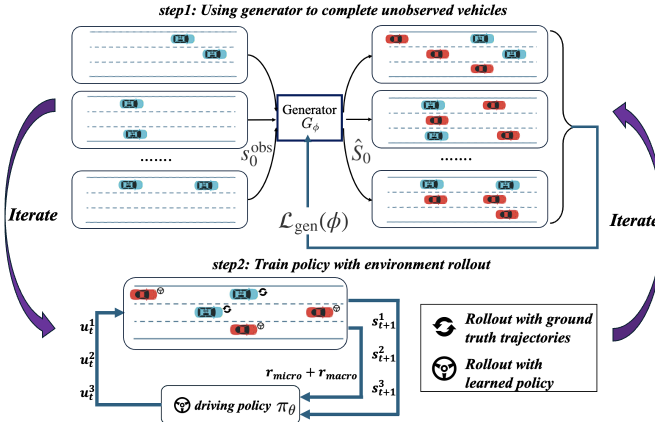


Fig. 2. Two-stage framework. Top (Step 1): the generator G_ϕ takes partial snapshots s_0^{obs} , completes hidden vehicles to form \hat{S}_0 , and is trained with the generator loss $\mathcal{L}_{\text{gen}}(\phi)$. Bottom (Step 2): episodes start from \hat{S}_0 ; the shared policy π_θ rolls out the environment and is updated using a trajectory-level score combining microscopic imitation r_{micro} and macroscopic alignment r_{macro} . In each simulation, observed vehicles follow their ground-truth trajectories, while unobserved vehicles are controlled by the learned policy.

served microscopic states from macroscopic observations and learns a shared policy whose rollouts are jointly consistent with individual demonstrations and aggregate measurements. Such frameworks should use available microscopic data to anchor observed individual behavior. Macroscopic statistics can then be used to constrain and regularize policies, promoting realistic flow patterns and safe coordination with human drivers at scale. Prior works on hybrid imitation learning and RL have begun to explore this direction [16], [25], but they typically assume either richly instrumented agents or idealized simulators and do not fully address learning from heterogeneous, partially observed real-world data streams.

A. Main Contributions

The main contributions of this work can be summarized into the following three aspects:

- **Problem formulation:** We aim to learn one shared driving policy using partial micro data and macro traffic summaries. The resulting policy should fit observed actions and reproduce aggregate statistics.
- **Two-stage solution:** We propose a two-stage policy training framework: (i) a generator that uses partial microscopic data and macroscopic statistics to generate unobserved ve-

hicles, and (ii) a RL policy learning scheme that trains a shared policy on these completed scenes so that its behavior matches individual demonstrations and reproduces the observed traffic statistics.

- **Case study:** We implement this framework in a ring-road case study with concrete generator and policy architectures, and show that the learned policy matches target speed and spacing statistics while producing realistic car-following trajectories at the microscopic level.

II. PRELIMINARIES AND PROBLEM FORMULATION

Before defining the shared driving policy, we introduce the basic traffic notation. We model traffic as a multi-agent dynamical system with a number N of vehicles indexed by $\mathcal{I} = \{1, \dots, N\}$. At time t , vehicle i has state $s_t^i \in \mathbb{R}^{d_s}$ and applies control $u_t^i \in \mathbb{R}^{d_u}$. The dynamics are $s_{t+1}^i = f(s_t^i, u_t^i; \omega)$, where f is the state update model and ω denotes model uncertainty. The joint microscopic state is $S_t = \{s_t^i\}_{i=1}^N$. Let the time index set be $\mathcal{T} = \{0, 1, \dots, T-1\}$. When clear from context, we omit the time subscript and write S for a generic state at $t \in \mathcal{T}$.

From the individual-vehicle perspective, a driving policy must depend on locally observable information. Let $O(S, i) \in \mathbb{R}^{d_o}$ be vehicle i 's observation (e.g., ego state and nearby vehicles). Each vehicle selects an action from its observation under a stochastic driving policy $\pi_\theta : S \mapsto u$. Given the common acknowledgment that behaviors are statistically aligned across vehicles [26]–[28], we posit a shared policy π_θ such that the action of any vehicle is $u^i = \pi_\theta(O(S, i))$ for all $i \in \mathcal{I}$. With the shared policy in place, we now describe the two complementary partial-data views used in this work: a microscopic view based on instrumented vehicles and a macroscopic view based on infrastructure sensing.

For the microscopic view, only a small subset of vehicles carries on-board sensors. We denote the index set of these instrumented vehicles by $\mathcal{I}_{\text{obs}} \subset \mathcal{I}$, where $|\mathcal{I}_{\text{obs}}| \ll N$ indicates that this subset is a small fraction of the N vehicles on the road. In other words, \mathcal{I}_{obs} collects the IDs of vehicles for which both observations and actions are available. The microscopic dataset is $\mathcal{D}_{\text{micro}} = \{(O(S, i), u^i) \mid i \in \mathcal{I}_{\text{obs}}\}$. Standard imitation learning fits a parameterized policy π_θ using only $\mathcal{D}_{\text{micro}}$, i.e., $\pi_\theta \in \arg \min_\theta \sum_{(o, u) \in \mathcal{D}_{\text{micro}}} d(\pi_\theta(o), u)$, where d denotes a pointwise discrepancy.

For the macroscopic view, infrastructure sensors provide scene-level aggregate measures of traffic behavior. We use a feature map $\Psi : S \rightarrow \mathbb{R}^p$ and write $\Psi(S)$ for descriptors such as mean speed, density, flow, and headway statistics over the road segment. These quantities are commonly obtained from loop detectors, radar, and cameras deployed on major corridors.

Together, these two sets of observations are complementary. $\mathcal{D}_{\text{micro}}$ supplies action-level supervision on an instrumented subset, while $\Psi(S)$ summarizes the full traffic stream.

Our goal is to learn a shared policy π_θ that is microscopically consistent with observed agent behavior and macroscop-

ically aligned with aggregate traffic statistics. Microscopic and macroscopic consistency as defined as follow:

- 1) Microscopically consistent on the observed vehicles means minimizing the distance between predicted and observed actions: $\min_{\theta} \sum_{i \in \mathcal{I}_{\text{obs}}} \sum_{t \in \mathcal{T}} d(\pi_{\theta}(O(S_t, i)), u_t^i)$, where $d(\cdot, \cdot)$ is a distance between the two actions.
- 2) Macroscopic consistency means that, when π_{θ} is followed population-wide, the induced trajectory $\{S_t^{\pi_{\theta}}\}_{t \in \mathcal{T}}$ matches the target aggregate statistics: $\min_{\theta} \sum_{t \in \mathcal{T}} d(\Psi(S_t^{\pi_{\theta}}), \Psi(S))$, where $d(\cdot, \cdot)$ is a distance between the two statistics.

In our case study, both microscopic and macroscopic consistency are enforced during training: the generator is optimized with $\mathcal{L}_{\text{gen}}(\phi)$, and the policy is trained with the trajectory-level objective $J(\theta)$.

To the best of our knowledge, jointly enforcing micro-macro alignment from heterogeneous, partially observed data has not been explicitly addressed and is challenging due to partial observability, identifiability, and multi-agent coupling.

III. PROPOSED SOLUTION

As mentioned in Section II, We aim to learn a shared policy π_{θ} from partially observed microscopic trajectories and macroscopic aggregates $\Psi(S)$ so that the learned behavior is microscopically consistent with observed actions and macroscopically aligned with target statistics when deployed population-wide.

As shown in Fig. 2, we realize this objective via a two-stage framework. A generator $G_{\phi} : (s_0^{\text{obs}}, \Psi(S)) \mapsto \hat{S}$ that reconstructs hidden microscopic states from partial observations and macroscopic statistics and a shared policy $\pi_{\theta} : S \mapsto u$ that enforces macro-micro alignment in closed-loop rollouts. We will further discuss two stages in detail.

A. Stage I: Generator for Hidden-State Completion

Goal. Given a partially observed snapshot s_0^{obs} and its aggregate descriptor $\Psi(S)$, the goal of this stage is to produce a completed initial state \hat{S}_0 using a learn-based generator G_{ϕ} .

Training. If we define the fully observed training scenes as $S_0 = \{s_0^i\}_{i \in \mathcal{I}}$, then the index set of observed vehicles is $\mathcal{I}_{\text{obs}} \subset \mathcal{I}$, and the index set of unobserved vehicles is $\mathcal{I}_{\text{hid}} = \mathcal{I} \setminus \mathcal{I}_{\text{obs}}$. For each scene we know the observed vehicle states $s_0^{\text{obs}} = \{s_0^i\}_{i \in \mathcal{I}_{\text{obs}}}$, while the unobserved vehicle states $s_0^{\text{hid}} = \{s_0^j\}_{j \in \mathcal{I}_{\text{hid}}}$ are unknown.

To reconstruct the full scene from partial information, we use the generator to map from the known part and the macroscopic descriptor to the hidden part, $\hat{s}_0^{\text{hid}} = G_{\phi}(s_0^{\text{obs}}, \Psi(S))$, and then form the completed state $\hat{S}_0 = (s_0^{\text{obs}}, \hat{s}_0^{\text{hid}})$. The generator is parameterized by ϕ and optimized via

$$\mathcal{L}_{\text{gen}}(\phi) = \lambda_{\text{macro}} d(\Psi(\hat{S}_0), \Psi(S)) + \lambda_{\text{rec}} d(\hat{s}_{t+1}^{\text{hid}}, s_{t+1}^{\pi_{\theta}, \text{hid}}) \quad (1)$$

where $\lambda_{\text{macro}}, \lambda_{\text{rec}} \geq 0$ are weighting coefficients. Here $s_{t+1}^{\pi_{\theta}, \text{hid}}$ denotes the hidden state at time $t+1$ obtained by rolling out the dynamics under the learned policy π_{θ} , i.e., $s_{t+1}^{\pi_{\theta}, \text{hid}} = f(s_t^{\text{hid}}, \pi_{\theta}(O(S_t)); \omega)$. The term $\hat{s}_{t+1}^{\text{hid}} = G_{\phi}(s_{t+1}^{\text{obs}}, \Psi(S))$ is

the generator's prediction of the same hidden state using the next-step observations and macroscopic descriptor. The reconstruction discrepancy $d(\hat{s}_{t+1}^{\text{hid}}, s_{t+1}^{\pi_{\theta}, \text{hid}})$ therefore encourages the generator's completions to stay consistent with the hidden states implied by the current policy, so that completed scenes and policy rollouts remain aligned over time. This consistency term is optional: it is only activated when we iteratively refine both the generator and the policy, and can be omitted, as is done in the case study in Section IV-B, if we do not perform such joint refinement. Detailed choices of the weights are reported in the case study.

B. Stage II: Policy Learning with Macro-Micro Consistency

Goal. Learn a shared policy π_{θ} that satisfies the microscopic and macroscopic consistency objectives in Section II.

Training. Unlike in the traditional RL learning paradigm, we evaluate the shared policy π_{θ} at the level of full rollouts rather than assigning rewards state by state. To be specific, we first initialize each episode from a generator-completed state \hat{S}_0 , and then roll out the dynamics under π_{θ} to obtain a trajectory $\tau = \{S_t\}_{t \in \mathcal{T}}$. On each trajectory τ , we define a microscopic score that measures how well the policy matches the observed actions on observed vehicles:

$$r_{\text{micro}}(\tau; \theta) = - \sum_{i \in \mathcal{I}_{\text{obs}}} \sum_{t \in \mathcal{T}} d(\pi_{\theta}(O(S_t, i)), u_t^i). \quad (2)$$

In parallel, we define a macroscopic score that measures how well the trajectory reproduces the target aggregate statistics:

$$r_{\text{macro}}(\tau; \theta) = - \sum_{t \in \mathcal{T}} D_{\text{macro}}(\Psi(S_t^{\pi_{\theta}}), \Psi(S)), \quad (3)$$

where $\Psi(S_t^{\pi_{\theta}})$ is the macroscopic feature of the simulated state at time t . The overall policy objective combines these two trajectory-level scores is then:

$$J(\theta) = \mathbb{E}_{\tau \sim (\pi_{\theta}, G_{\phi})} [r_{\text{micro}}(\tau; \theta) + \eta r_{\text{macro}}(\tau; \theta)], \quad (4)$$

where $\eta \geq 0$ controls the relative weight of macroscopic alignment. We optimize θ to maximize $J(\theta)$ using policy-gradient or actor-critic updates over batches of rollouts, so that each update reflects the aggregated macro-micro performance of the entire policy, rather than treating individual transitions in isolation. The entire procedure is summarized in Algorithm 1.

IV. EXPERIMENT AND CASE STUDY

To further illustrate our proposed solution, we instantiate the general formulation in a controlled ring-road environment. Consider a circular single-lane roadway with radius R and N vehicles moving in the same direction. The microscopic state of vehicle at time t is $s_t^i = (\theta_t^i, v_t^i)$ where $\theta_t^i \in [0, 2\pi]$ is the angular position and $v_t^i \in [10.5, 14] \text{m/s}$ is the velocity.

From fully observed ring-road trajectories, we instantiate the macroscopic descriptor as $\Psi(S) = [\bar{v}_{\text{GT}}, \bar{d}, d_{\min}, d_{\max}, v_{\min}, v_{\max}]$, where \bar{v}_{GT} is the fleet-average speed, \bar{d} is mean spacing between two close vehicles, and (d_{\min}, d_{\max}) and (v_{\min}, v_{\max}) are admissible spacing and

Algorithm 1 Two-stage policy learning framework

- 1: **Stage I: Train G_ϕ**
- 2: **while** not converged (validation generator loss \mathcal{L}_{gen} (Eqs. (1)) does not improve by ε for sufficient number of epochs, or max steps reached) **do**
- 3: Sample fully observed snapshot S_0 .
- 4: Choose \mathcal{I}_{obs} , set $\mathcal{I}_{\text{hid}} = \mathcal{I} \setminus \mathcal{I}_{\text{obs}}$.
- 5: Form s_0^{obs} , s_0^{hid} , compute $\Psi(S) = \Psi(S_0)$.
- 6: Predict $\hat{s}_0^{\text{hid}} = G_\phi(s_0^{\text{obs}}, \Psi(S))$; set $\hat{S}_0 = (s_0^{\text{obs}}, \hat{s}_0^{\text{hid}})$.
- 7: Update ϕ using $\mathcal{L}_{\text{gen}}(\phi)$ (Eqs. (1)).
- 8: **end while**
- 9: **Stage II: Train π_θ with fixed G_ϕ .**
- 10: **while** not converged (policy objective $J(\theta)$ (Eqs. (4)) does not improve by ε for sufficient number of steps, or max steps reached) **do**
- 11: Sample partially observed snapshot s_0^{obs} and $\Psi(S)$.
- 12: Build $\hat{S}_0 = (s_0^{\text{obs}}, G_\phi(s_0^{\text{obs}}, \Psi(S)))$.
- 13: Initialize $S_0 \leftarrow \hat{S}_0$; simulate a rollout of length H under π_θ to obtain trajectory τ .
- 14: Compute $r_{\text{micro}}(\tau; \theta)$ and $r_{\text{macro}}(\tau; \theta)$ (Eqs. (2)–(3)).
- 15: Update θ to maximize $J(\theta)$ (Eqs. (4)).
- 16: **end while**
- 17: **Optional:** Repeat Stage I and Stage II in a few outer iterations until performance saturates.
- 18: **Output:** Trained generator G_ϕ and shared policy π_θ .

speed bounds. These quantities form the macroscopic targets used in the generator loss and in the macroscopic consistency term of the policy objective.

For this case study, each controllable vehicle uses the local observation $o_t^i = [v_t^i, v_{\text{limit}}(\theta_t^i), d_{\text{pre},t}^i, \Delta v_t^i]$, where $v_{\text{limit}}(\theta_t^i)$ is the local speed limit along the ring, $d_{\text{pre},t}^i$ is the headway to the preceding vehicle in angular order, and Δv_t^i is the relative speed to that preceding vehicle.

The control input coincides with the generic action u_t^i and is given by $u_t^i \in [a_{\min}, a_{\max}]$ with fixed longitudinal acceleration bounds $a_{\min} = -1.1$ and $a_{\max} = 0.5$.

Under this ring-road setup and given partially observed scenes s_t^{obs} and macroscopic targets $\Psi(S)$, the general objective in Section II becomes: (i) to learn a generator G_ϕ that reconstructs plausible full states \hat{S}_t , and (ii) to learn a shared policy π_θ whose closed-loop behavior is microscopically safe and macroscopically consistent.

A. Data Collection

To obtain fully observed training data for this case study, we simulate traffic on the ring using the Intelligent Driver Model (IDM) [17] as the underlying car-following rule.

For each simulation run, N vehicles are initialized with randomized angular positions and speeds away from steady state. IDM parameters are independently sampled from prescribed ranges to induce heterogeneous behaviors. Across runs, piecewise-constant speed limits $v_{\text{limit}}(\theta)$ are randomized along the ring to create spatially varying operating conditions. This

prevents convergence to a trivial homogeneous equilibrium and yields diverse, realistic car-following and spacing patterns.

B. Generator Architecture and Autoregressive Rollout

In the ring-road case study, we instantiate the generator G_ϕ with a lightweight autoregressive model that operates on the microscopic state $S_t = \{(\theta_t^i, v_t^i)\}_{i=1}^N$. To be more specific, given a partially observed snapshot s_0^{obs} and macroscopic descriptor $\Psi(S)$, the generator is trained to produce a completed state $\hat{S}_0 = (s_0^{\text{obs}}, \hat{s}_0^{\text{hid}})$ via $\hat{s}_0^{\text{hid}} = G_\phi(s_0^{\text{obs}}, \Psi(S))$.

To train the generator, we instantiate the discrepancy as $d(\Psi(\hat{S}_0), \Psi(S)) = \lambda_v L_{\text{speed}} + \lambda_d L_{\text{dist}}$. Thus, the generator is trained with

$$\mathcal{L}_{\text{gen}}(\phi) = \lambda_v L_{\text{speed}} + \lambda_d L_{\text{dist}} \quad (5)$$

where λ_v, λ_d are scalar weights reported in the case study. Then we introduced the specific loss term. The fleet-average speed term is $L_{\text{speed}} = \left(\frac{1}{N} \sum_{i=1}^N v_i - \bar{v}_{\text{GT}} \right)^2$. When policy generated hidden states are available, we add $L_{\text{rec}} = \frac{1}{K} \sum_{j \in \mathcal{I}_{\text{hid}}} \|\hat{s}_0^j - s_0^j\|_2^2$. Spacing is enforced by a composite penalty $L_{\text{dist}} = L_{\text{mean}} + L_{\text{min}} + L_{\text{max}} + L_{\text{var}}$. Here \mathcal{A} indexes gaps influenced by generated vehicles. The mean-gap term is $L_{\text{mean}} = \left(\frac{1}{|\mathcal{A}|} \sum_{i \in \mathcal{A}} d_i - \bar{d} \right)^2$. Lower-bound violations use $L_{\text{min}} = \frac{1}{|\mathcal{A}|} \sum_{i \in \mathcal{A}} \left(\frac{\max(0, d_{\min} - d_i)}{d_{\min}} \right)^2$. Upper-bound violations use $L_{\text{max}} = \frac{1}{|\mathcal{A}|} \sum_{i \in \mathcal{A}} \left(\frac{\max(0, d_i - d_{\max})}{d_{\max}} \right)^2$. Dispersion is controlled by $L_{\text{var}} = \text{std}(\{d_i\}_{i \in \mathcal{A}})/\bar{d}$. Together, these terms align the generator with ideal spacing and speed. Generator training for ring-road case study is summarized in Algorithm 2.

Algorithm 2 Generator training in the ring-road case study

Require: Training pairs (s_0^{obs}, S_0) on the ring road; vehicle index set \mathcal{I} ; descriptor $\Psi(S) = [\bar{v}_{\text{GT}}, \bar{d}, d_{\min}, d_{\max}, v_{\min}, v_{\max}]$; weights λ_v, λ_d .

- 1: Initialize generator parameters ϕ .
- 2: **for** each training iteration **do**
- 3: Sample one initial observed state from dataset s_0^{obs} .
- 4: Complete the hidden states $\hat{s}_0^{\text{hid}} = G_\phi(s_0^{\text{obs}}, \Psi(S))$. Form the completed state $\hat{S}_0 = (s_0^{\text{obs}}, \hat{s}_0^{\text{hid}})$.
- 5: Compute the generator loss $\mathcal{L}_{\text{gen}}(\phi)$ (Eqs. (5)) .
- 6: Update ϕ by one gradient step on $\mathcal{L}_{\text{gen}}(\phi)$.
- 7: **end for**

During generator inference, given a partially observed frame with K hidden vehicles, we complete the scene via an autoregressive rollout with hard-constraint rejection. At step $s = 1, \dots, K$, the generator proposes $(\hat{\theta}^{(s)}, \hat{v}^{(s)})$ given the observed state. We accept the candidate only if it satisfies the distance and velocity bounds $[d_{\min}, d_{\max}]$ and $[v_{\min}, v_{\max}]$. Otherwise, we resample up to T_{\max} trials. If none is feasible, we project the last candidate to the nearest feasible bounds. This yields collision-free, macro-consistent completions while keeping observed vehicles unchanged. Generator inference for ring-road case study is summarized in Algorithm 3.

Algorithm 3 Generator inference in the ring-road case study

```

Require: Trained  $G_\phi$ ; partially observed snapshot  $s_0^{\text{obs}}$ ; descriptor  $\Psi(S)$ ; bounds  $[d_{\min}, d_{\max}]$ ,  $[v_{\min}, v_{\max}]$ ; max trials  $T_{\max}$ ; hidden count  $K$ .
1: Initialize  $\hat{S}_0 \leftarrow s_0^{\text{obs}}$ .
2: for  $s = 1$  to  $K$  do
3:   accepted  $\leftarrow$  false.
4:   for  $t = 1$  to  $T_{\max}$  do
5:     Propose a candidate  $(\hat{\theta}^{(s)}, \hat{v}^{(s)}) = G_\phi(\hat{S}_0, \Psi(S))$ .
6:     Tentatively insert  $(\hat{\theta}^{(s)}, \hat{v}^{(s)})$  into  $\hat{S}_0$  and compute the affected gaps  $d$ .
7:     if all  $d \in [d_{\min}, d_{\max}]$  and  $\hat{v}^{(s)} \in [v_{\min}, v_{\max}]$  then
8:       Accept the candidate and update  $\hat{S}_0$ ; set accepted  $\leftarrow$  true;
9:       break.
10:    end if
11:   end for
12:   if not accepted then
13:     break {If no feasible candidate is found after  $T_{\max}$  trials}
14:   end if
15: end for
15: Return  $\hat{S}_0$ .

```

C. Policy Architecture

Episodes are initialized from generator-completed states \hat{S}_0 and rolled out under the shared policy π_θ to produce trajectories $\tau = \{S_t\}_{t \in \mathcal{T}}$. We reuse the macroscopic penalties $L_{\text{speed},t}$ and $L_{\text{dist},t}$ exactly as defined before, and score an entire policy by aggregating over full rollouts.

We evaluate each rollout with two complementary terms and combine them into a single objective. From the microscopic perspective, on a trajectory τ we score agreement with instrumented actions by accumulating their log-likelihood under the policy using $r_{\text{micro}}(\tau; \theta) = \sum_{i \in \mathcal{I}_{\text{obs}}} \sum_{t \in \tau} \log \pi_\theta(u_t^i \mid O(S_t, i))$. From the macroscopic perspective, to encourage aggregate alignment at each step we map the speed/spacing penalties to a bounded reward $r_{\text{macro}}(\tau; \theta) = \sum_{t \in \tau} r_{\text{macro},t}$ with $r_{\text{macro},t} = (1 + \lambda_v L_{\text{speed},t} + \lambda_d L_{\text{dist},t})^{-1}$ and aggregate over time. The policy maximizes the trajectory-level score $J(\theta) = \mathbb{E}_{\tau \sim (\pi_\theta, G_\phi)} [r_{\text{micro}}(\tau; \theta) + \eta r_{\text{macro}}(\tau; \theta)]$, where $\eta \geq 0$ balances the two terms. We maximize $J(\theta)$ with Proximal Policy Optimization (PPO) [29] using a value-function baseline and generalized advantage estimation. PPO operates on batches of trajectories initialized by G_ϕ and uses the clipped surrogate objective. Detailed hyperparameters are provided in Table I.

V. RESULTS AND DISCUSSIONS

On the ring-road case study, we demonstrate that our two-stage pipeline learns a shared policy that fuses partial microscopic traces with infrastructure-level aggregates. The resulting policy is aligned with the target behavior both macroscopically and microscopically.

1) *Macroscopic Alignment*: We first evaluate whether generator-completed scenes and the learned policy preserve the aggregate traffic statistics defined in Section IV.

We analysis the mean and standard deviation of longitudinal speed and distance to the preceding vehicle using the same

TABLE I
CASE STUDY HYPERPARAMETERS

Hyperparameter	Symbol	Value
Ring radius	R	100 m
Vehicle count	N	5
Speed range	$[v_{\min}, v_{\max}]$	[10.5, 14.0] m/s
Target fleet-average speed	\bar{v}_{GT}	12.06 m/s
Target mean spacing	\bar{d}	126 m
Spacing bounds	$[d_{\min}, d_{\max}]$	[115, 140] m
Acceleration bounds	$[a_{\min}, a_{\max}]$	[-1.1, 0.5] m/s ²
Hidden vehicles per frame	K	[0, 5]
Max trials per hidden	T_{\max}	20
Speed penalty weight	λ_v	0.5
Spacing penalty weight	λ_d	0.5
Macro reward weight	η	0.3
Trajectory horizon	H	10

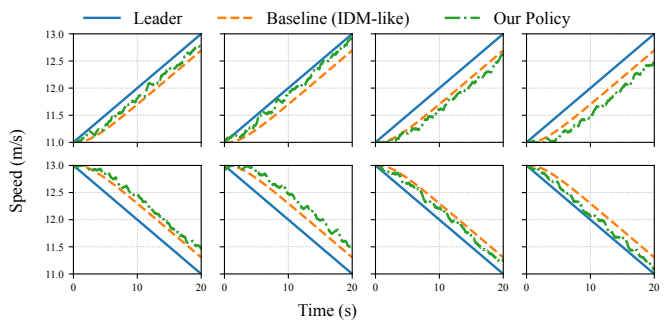


Fig. 3. Leader-follower velocity profiles in two scenarios. Top: leader accelerates 11m/s \rightarrow 13 m/s; bottom: leader decelerates 13m/s \rightarrow 11 m/s. In these plots, the velocity trajectories are drawn in green (leader), blue (ground-truth IDM follower), and orange (our learned policy follower), respectively. Across runs, the policy's average profile follows the ground-truth trend.

simulation settings. For simulation rollouts, we choose the number of unobserved vehicle to be $K = 1\text{--}4$ per scenario.

For unobserved counts $K \in \{1, 2, 3, 4\}$, the learned policy maintains a mean speed close to the ground-truth mean of 12.06 m/s, yielding 11.55, 11.54, 11.52, and 11.53 m/s, respectively; the largest absolute deviation is 0.54 m/s. The speed standard deviation increases from 0.37 m/s (ground-truth) to 0.78–0.80 m/s. The mean spacing remains 125.66 m for all K . The spacing standard deviation changes only slightly, from 34.60 m (ground-truth) to at most 34.79 m, an increase of 0.19 m.

Across all values of K , the mean speeds remain close to the ground-truth value and the spacing statistics stay essentially unchanged, while the increases in variance are mild. This shows that the generator reconstructs hidden vehicles without distorting macroscopic density, and that the learned policy, operating on these completions, maintains realistic macroscopic behavior under partial observations.

2) *Microscopic Behavior of the Learned Policy*: We next examine whether the learned policy exhibits meaningful microscopic responses consistent with the macroscopic alignment. To analyze its driving behavior, we construct two leader-follower scenarios in which the leader either accelerates or decelerates according to a prescribed velocity profile. In each scenario, the lead vehicle follows this fixed profile, while the following vehicle is controlled by either the ground-truth

IDM-based policy or our learned policy. The follower starts 126 m behind the leader and shares the same initial speed.

Fig. 3 visualizes representative leader-follower trials under leader acceleration-only and leader deceleration-only scenarios. The learned policy does not exactly replicate the IDM trajectory, but its responses are coherent: it accelerates and decelerates in the appropriate phases, maintains safe headways, and avoids unrealistic gap collapse or divergence.

Over multiple trials, some sampled trajectories lie slightly above the ground-truth velocity profile and some lie slightly below, in both acceleration-only and deceleration-only scenarios. This variability is structured and physically plausible, rather than noisy. As a result, when aggregating over trials, the ensemble of rollouts matches the target macroscopic statistics in both mean and dispersion. In other words, the policy is macroscopically aligned precisely because its microscopic behaviors form a balanced family of realistic car-following patterns, rather than collapsing to a single deterministic trace.

Together, the macroscopic statistics and shared policy analysis demonstrate that the proposed generator-policy pipeline is macroscopically consistent and microscopically meaningful. It preserves aggregate traffic statistics while producing plausible local interactions that explain those statistics.

VI. CONCLUSION AND FUTURE WORK

In this paper, we have presented a macro-micro framework for learning a shared driving policy from heterogeneous traffic data, combining partially observed microscopic trajectories with macroscopic statistics. The approach uses a generator to complete hidden vehicle states and a shared policy trained on these completed scenes to achieve consistency with both individual behaviors and aggregate traffic patterns. We have demonstrated the approach in a simple controlled ring-road case study. Future work will focus on extending this framework to multi-lane roads, intersections, and network-scale settings with richer heterogeneity. Methods will be further evaluated using real-world datasets that provide both infrastructure-level measurements and subset-based microscopic trajectories within the same environment.

REFERENCES

- [1] C. Chen, A. Seff, A. Kornhauser, and J. Xiao, “Deepdriving: Learning affordance for direct perception in autonomous driving,” in *Proceedings of the IEEE international conference on computer vision*, 2015, pp. 2722–2730.
- [2] M. Bojarski, D. Del Testa, D. Dworakowski, B. Firner, B. Flepp, P. Goyal, L. D. Jackel, M. Monfort, U. Muller, J. Zhang *et al.*, “End to end learning for self-driving cars,” in *Conference on Computer Vision and Pattern Recognition Workshops*, 2016.
- [3] H. Xu, Y. Gao, F. Yu, and T. Darrell, “End-to-end learning of driving models from large-scale video datasets,” in *Proceedings of the IEEE conference on computer vision and pattern recognition*, 2017, pp. 2174–2182.
- [4] Y. Hu, J. Yang, L. Chen, K. Li, C. Sima, X. Zhu, S. Chai, S. Du, T. Lin, W. Wang *et al.*, “Planning-oriented autonomous driving,” in *Proceedings of the IEEE/CVF Conference on Computer Vision and Pattern Recognition*, 2023, pp. 17853–17862.
- [5] T. Han, J. Jing, and Ü. Özgürer, “Driving intention recognition and lane change prediction on the highway,” in *2019 IEEE Intelligent Vehicles Symposium (IV)*. IEEE, 2019, pp. 957–962.
- [6] M. Bojarski, P. Yeres, A. Choromanska, K. Choromanski, B. Firner, L. Jackel, and U. Muller, “Explaining how a deep neural network trained with end-to-end learning steers a car,” *arXiv preprint arXiv:1704.07911*, 2017.
- [7] F. Codevilla, M. Müller, A. López, V. Koltun, and A. Dosovitskiy, “End-to-end driving via conditional imitation learning,” in *2018 IEEE International Conference on Robotics and Automation (ICRA)*, pp. 4693–4700, 2018.
- [8] J. Hawke, R. Shen, C. Gurau, S. Sharma, D. Reda, N. Nikolov, P. Mazur, S. Micklethwaite, N. Griffiths, A. Shah *et al.*, “Urban driving with conditional imitation learning,” in *2020 IEEE International Conference on Robotics and Automation (ICRA)*. IEEE, 2020, pp. 251–257.
- [9] J. Chen, Z. Wang, and M. Tomizuka, “Deep hierarchical reinforcement learning for autonomous driving with distinct behaviors,” in *2018 IEEE intelligent vehicles symposium (IV)*. IEEE, 2018, pp. 1239–1244.
- [10] E. Sonu, Z. Sunberg, and M. J. Kochenderfer, “Exploiting hierarchy for scalable decision making in autonomous driving,” in *2018 IEEE Intelligent Vehicles Symposium (IV)*. IEEE, 2018, pp. 2203–2208.
- [11] A. Geiger, P. Lenz, and R. Urtasun, “Are we ready for autonomous driving? the kitti vision benchmark suite,” in *2012 IEEE Conference on Computer Vision and Pattern Recognition (CVPR)*. IEEE, 2012, pp. 3354–3361.
- [12] B. Paden, M. Čáp, S. Z. Yong, D. Yershov, and E. Frazzoli, “A survey of motion planning and control techniques for self-driving urban vehicles,” *IEEE Transactions on Intelligent Vehicles*, vol. 1, no. 1, pp. 33–55, 2016.
- [13] D. Helbing, “Traffic and related self-driven many-particle systems,” *Reviews of modern physics*, vol. 73, no. 4, p. 1067, 2001.
- [14] A. Kendall, J. Hawke, D. Janz, P. Mazur, D. Reda, J.-M. Allen, V.-D. Lam, A. Bewley, and A. Shah, “Learning to drive in a day,” in *2019 International Conference on Robotics and Automation (ICRA)*. IEEE, 2019, pp. 8248–8254.
- [15] E. Yurtsever, J. Lambert, A. Carballo, and K. Takeda, “A survey of autonomous driving: Common practices and emerging technologies,” *IEEE access*, vol. 8, pp. 58443–58469, 2020.
- [16] B. R. Kiran, I. Sobh, V. Talpaert, P. Mannion, A. A. Al Sallab, S. Yoganmani, and P. Pérez, “Deep reinforcement learning for autonomous driving: A survey,” *IEEE Transactions on Intelligent Transportation Systems*, vol. 23, no. 6, pp. 4909–4926, 2021.
- [17] M. Treiber, A. Hennecke, and D. Helbing, “Congested traffic states in empirical observations and microscopic simulations,” *Physical review E*, vol. 62, no. 2, p. 1805, 2000.
- [18] Traffic Technology Today, “V2X OBU deployed in New York’s CV pilot,” *Traffic Technology Today*, 2019. [Online]. Available: <https://www.traffictechnologytoday.com/news/connected-vehicles/v2x-obu-deployed-in-new-yorks-cv-pilot.html>
- [19] I. D. Evaluation, “The connected electric automated vehicle pilot in columbus, ohio improved the last mile mobility of goods, delivering 129,528 meals to the community over the eight-month pilot,” *ITS Deployment Evaluation*, 2022. [Online]. Available: <https://www.itskrs.its.dot.gov/>
- [20] T. T. Today, “Ohio to establish center for smart mobility to further cav development programs,” *Traffic Technology Today*, 2018. [Online]. Available: <https://www.traffictechnologytoday.com/news/autonomous-vehicles/ohio-to-establish-center-for-smart-mobility-to-further-cav-development-programs.html>
- [21] U. D. of Transportation, “Interactive connected vehicle deployment map,” *US Department of Transportation*, 2023. [Online]. Available: <https://www.transportation.gov/av/cv-pilot-deployment-program>
- [22] Verizon Connect, “2024 fleet technology trends report,” https://www.datocms-assets.com/992/1698962079-vzc-2077702-2024-fleet-technology-trends_final_digital.pdf, 2024, accessed: 2024-08-27.
- [23] N. Djuric, V. Radosavljevic, F.-C. Chou, T.-H. Lin, E. Vlahogianni, and J. Wang, “Short-term motion prediction of traffic actors for autonomous driving using deep convolutional networks,” *arXiv preprint arXiv:1808.05819*, 2018.
- [24] X. Chen, H. Ma, J. Wan, B. Li, and T. Xia, “Deep multi-modal object detection and semantic segmentation for autonomous driving: Datasets, methods, and challenges,” *IEEE Transactions on Intelligent Transportation Systems*, vol. 21, no. 7, pp. 2933–2945, 2019.
- [25] W. Zhang and Y. Gao, “Robustness of deep reinforcement learning for autonomous driving in dense traffic scenarios,” *IEEE Transactions on Intelligent Vehicles*, vol. 6, no. 4, pp. 565–575, 2021.

- [26] D. Helbing, A. Hennecke, V. Shvetsov, and M. Treiber, “Micro-and macro-simulation of freeway traffic,” *Mathematical and computer modelling*, vol. 35, no. 5-6, pp. 517–547, 2002.
- [27] A. Kesting and M. Treiber, “Calibrating car-following models by using trajectory data: Methodological study,” *Transportation Research Record*, vol. 2088, no. 1, pp. 148–156, 2008.
- [28] M. Treiber and A. Kesting, “Car-following models based on driving strategies,” in *Traffic flow dynamics: Data, models and simulation*. Springer, 2025, pp. 239–284.
- [29] J. Schulman, F. Wolski, P. Dhariwal, A. Radford, and O. Klimov, “Proximal policy optimization algorithms,” *arXiv preprint arXiv:1707.06347*, 2017.